

Plasmonic-MZM-based Short-Reach Transmission up to 10 km Supporting >304 GBd Polybinary or 432 Gbit/s PAM-8 Signaling

Conference Paper

Author(s):

Hu, Qian; Borkowski, Robert; Lefevre, Yannick; Buchali, Fred; Bonk, René; Schuh, Karsten; De Leo, Eva; Habegger, Patrick; Destraz, Marcel; Del Medico, Nino; Duran, Hamit; Tedaldi, Valentino; Funck, Christian; Fedoryshyn, Yuriy; [Leuthold, Juerg](#) ; [Henri, Wolfgang](#) ; [Bäuerle, Benedikt](#) ; Hoessbacher, Claudia

Publication date:

2021

Permanent link:

<https://doi.org/10.3929/ethz-b-000528337>

Rights / license:

[In Copyright - Non-Commercial Use Permitted](#)

Originally published in:

<https://doi.org/10.1109/ecoc52684.2021.9606060>

Plasmonic-MZM-based Short-Reach Transmission up to 10 km Supporting >304 GBd Polybinary or 432 Gbit/s PAM-8 Signaling

Qian Hu⁽¹⁾, Robert Borkowski⁽¹⁾, Yannick Lefevre⁽²⁾, Fred Buchali⁽¹⁾, René Bonk⁽¹⁾, Karsten Schuh⁽¹⁾, Eva De Leo⁽³⁾, Patrick Habegger⁽³⁾, Marcel Destraz⁽³⁾, Nino Del Medico⁽³⁾, Hamit Duran⁽³⁾, Valentino Tedaldi⁽³⁾, Christian Funck⁽³⁾, Yuriy Fedoryshyn⁽⁴⁾, Juerg Leuthold^(3,4), Wolfgang Heni⁽³⁾, Benedikt Baeuerle⁽³⁾, Claudia Hoessbacher⁽³⁾

(1) Nokia, Lorenzstr. 10, 70435 Stuttgart, Germany qian.hu@nokia-bell-labs.com

(2) Nokia, Copernicuslaan 50, 2018 Antwerp, Belgium

(3) Polariton Technologies Ltd., 8803 Rüslikon, Switzerland

(4) ETH Zürich, Institute of Electromagnetic Fields (IEF), 8092 Zürich, Switzerland

Abstract We employ an ultrabroad-bandwidth plasmonic Mach-Zehnder modulator to demonstrate 10-km IM/DD transmission at a symbol rate of 304-GBd (AIR 293.3-Gbit/s, net 270.0-Gbit/s) realized with a polybinary modulation scheme, and a line rate of 432-Gbit/s (AIR 383.6-Gbit/s, net 350.4-Gbit/s) using PAM-8.

Introduction

Driven by the enormous cloud expansion, future standards for short-reach datacenter interconnects (DCIs) will aim at beyond-800G optics (e.g., 1.6TbE^[1]). Stringent transceiver cost targets favor intensity modulation and direct detection (IM/DD), but simultaneously lanes at 200 Gbit/s and beyond are needed to support future bandwidth needs of up to 10 km DCIs^[2,3]. The key element of a next generation short-reach system is an optical modulator with a high electro-optical (EO) bandwidth and a small footprint. The former characteristic is necessary to keep a small number of parallel lanes while increasing the total data rate of the optical interface, thus enabling low complexity chips with low power consumption; the latter is essential to achieve a high degree of integration and a high faceplate density in case of pluggable form factors.

A variety of modulator technologies enabling >100 GHz EO bandwidths have been reported^[4-7]. A plasmonic Mach-Zehnder modulator (MZM), which can offer an EO bandwidth beyond 500 GHz^[8] and a micron-scale footprint, is promising for future ultrahigh-speed optical transmission. To date, the highest rate demonstrated using such modulator was 222 GBd on-off keying (OOK) at a net bitrate of 177.6 Gbit/s^[7].

The plasmonic MZM relies on standard passive silicon photonics components built on a

silicon-on-insulator wafer^[9]. In the active area, standard *p-n* junctions are replaced by plasmonic-organic hybrid (POH) phase shifters that utilize the Pockels effect^[10]. Thanks to sub-diffraction light confinement in the POH phase shifter, only a 15- μm -long active area is required. These micron-scale dimensions provide a two-fold benefit: (i) small capacitances, which result in small RC constants, boosting the switching speed; (ii) negligible walk-off between electrical and optical waves. The active material of the plasmonic MZM allows for operation in the wavelength range spanning from 1.2 μm to 1.6 μm ^[11], however, the specific device under test is restricted to C-band operation due to the bandwidth limit of the grating couplers. Nonetheless, O-band operation could be possible with a different coupler design, promising ultrafast transmission over dispersion uncompensated DCIs. A photograph of the packaged device used in this experiment, fitted with a 1 mm connector, is shown in Fig. 1(b).

In this work we employ this plasmonic MZM to experimentally demonstrate its capabilities in terms of high-symbol-rate multilevel IM. Transmission over 2.5 km and 10 km standard single-mode fiber (SSMF) is demonstrated, applying various modulation formats, including multi-level pulse amplitude modulation (PAM) signals, simple OOK (binary) modulation, as well

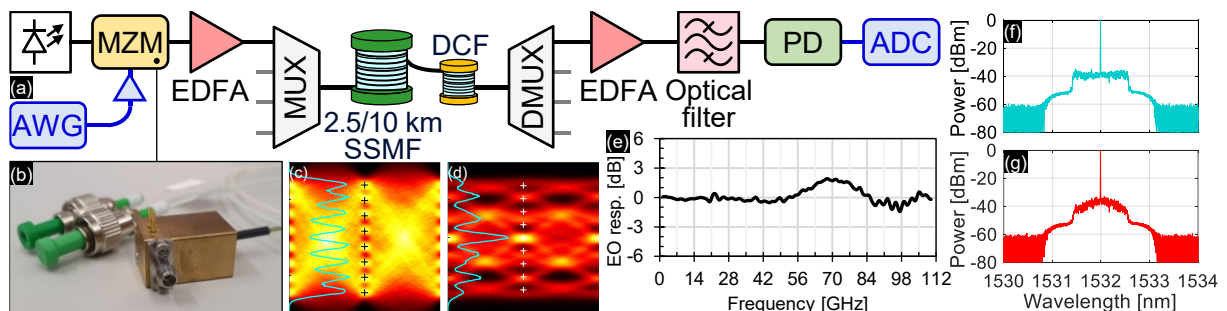


Fig. 1: (a) Experimental demonstration of ultrahigh-symbol-rate IM/DD system. (b) Photograph of the tested modulator. (c,d) Eye diagrams of the equalized (c) 144 GBd PAM-8 and (d) 240 GBd tetrabinary signals at the receiver. (e) EO response of the modulator under test. (f,g) Optical spectra of the transmitted (f) 160 GBd PAM-4 and (g) 280 GBd tetrabinary signals.

as partial-response-encoded binary (polybinary) signals^[12], where short (at most 4 symbols), controlled inter-symbol interference (ISI) is induced for spectral shaping, allowing for limited-complexity decoder on the receiver side. A symbol rate of 304 GBd is demonstrated with a polybinary modulation scheme, yielding, after 10 km of SSMF, an achievable information rate (AIR) of 293.3 Gbit/s, and a net bitrate of 274 Gbit/s. Compared to the previous plasmonic-MZM-based IM/DD demonstration^[7], the symbol rate is increased by 36.9%. With PAM-8 signal, a line rate of 432 Gbit/s is achieved at 144 GBd, resulting in an AIR of 383.6 Gbit/s, and a net bitrate of 350.4 Gbit/s after 10 km of SSMF, almost double the previously reported net bitrate with this type of modulator^[7].

Experimental demonstration

Fig. 1(a) shows the experimental setup. The MZM has a static extinction ratio of >28 dB, a V_π of 8.3 V, and a fiber-to-fiber insertion loss of <18 dB. Fig. 1(e) shows the EO frequency response of this modulator, which remains around 0 dB up to 110 GHz. The electrical signal fed into the plasmonic MZM is generated from a 256 GSa/s arbitrary waveform generator (AWG) with ≈ 65 GHz 3-dB analog bandwidth followed by an 11 dB driver amplifier with ≈ 70 GHz bandwidth. The overall bandwidth of the modulated signal after applying pre-emphasis is ≈ 72 GHz. The MZM itself is not pre-emphasized due to its >110 GHz bandwidth. A laser source emitting at 1532 nm provides an optical carrier up to 10 dBm to the modulator. Its output is connected to an erbium-doped fiber amplifier (EDFA) followed by a programmable optical filter, which acts as a channel multiplexer with a 2 nm fourth-order super-Gaussian transfer function. The optical launch power is 9.5 dBm. The optical signal is tested back-to-back and transmitted over 2.5 km or 10 km standard single-mode fiber (SSMF), while the dispersion accumulated in the fiber link is compensated by a dispersion compensating fiber (DCF). At the receiver, another optical filter, acting as a channel demultiplexer, is used. The received optical signal is amplified with an EDFA, passes through a 1.5 nm optical filter and is detected using a 100 GHz *p-i-n* photodiode (PD). The input power for the PD is 6.5 dBm. The electrical signal is sampled by a free-running 256 GSa/s analog-to-digital converter (ADC) with an 84 GHz anti-aliasing brick-wall filter.

For *M*-level PAM transmission, symbols are upsampled to 256 GSa/s and pulse-shaped using a raised-cosine filter with a roll-off of 0.1. In the receiver DSP, the signal is resampled to 2 samples/symbol (Sps) and filtered to remove out-of-band noise. Next, a $T/2$ -spaced nonlinear feedforward equalizer (FFE) concatenated with a

T -spaced decision feedback equalizer (DFE) is applied. Potential phase drifts between the unsynchronized clocks of the transmitter and the receiver are compensated within the adaptive equalizer. The equalized 144 GBd PAM-8 signal has an eye diagram shown in Fig. 1(c). After equalization, the signal is decimated to 1 Sps to evaluate the normalized generalized mutual information (NGMI) assuming Gray labeling. The computation of AIR, as well as thresholds of practical soft-decision forward error correction (FEC) codes, used to extract net bitrate, are explained in the following section.

To achieve higher symbol rates, polybinary modulation with spectral shaping is employed. A polybinary signal is generated by convolving a binary signal with an impulse response $(1 + z^{-1})^n$, where $n \in \{1,2,3\}$, which corresponds to, respectively, duobinary, tribinary and tetrabinary signaling. Such an encoded signal is then resampled to 256 GSa/s. Symbol rates higher than AWG sampling rate can be achieved for high-order polybinary signals since the polybinary filter shifts the spectral energy closer to zero frequency^[12]. The receiver DSP is similar as the one applied to PAM signals. Equalizer at the receiver targets a multi-level signal corresponding to the impulse response $(1 + z^{-1})^n$. The eye diagram of the equalized 240 GBd tetrabinary is shown in Fig. 1(d). A low-complexity Bahl-Cocke-Jelinek-Raviv (BCJR) algorithm with a small number of states equal to 2^n is then used to decode the polybinary signal back to the binary sequence. BCJR outputs log-likelihood ratios (LLRs), which are subsequently used for computation of the NGMI metric. Alternatively, bit decision can be made based on the LLR sign, therefore BER can also be computed.

Results for PAM modulation

The performance of PAM-4 and PAM-8 transmission is measured in a wide range of symbol rates. The obtained NGMI is plotted as a function of symbol rate as shown in Fig. 2(a). The AIR in Fig. 2(b) is computed from NGMI as $AIR = NGMI \cdot R_s \log_2(M)$, where R_s is the symbol rate

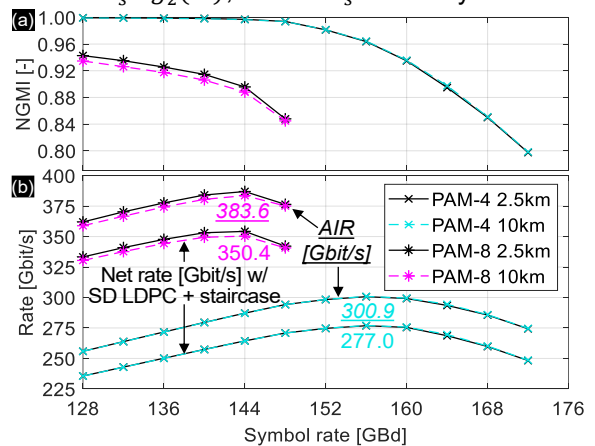


Fig. 2: (a) NGMI; (b) AIR and net bitrates for PAM-4 and PAM-8.

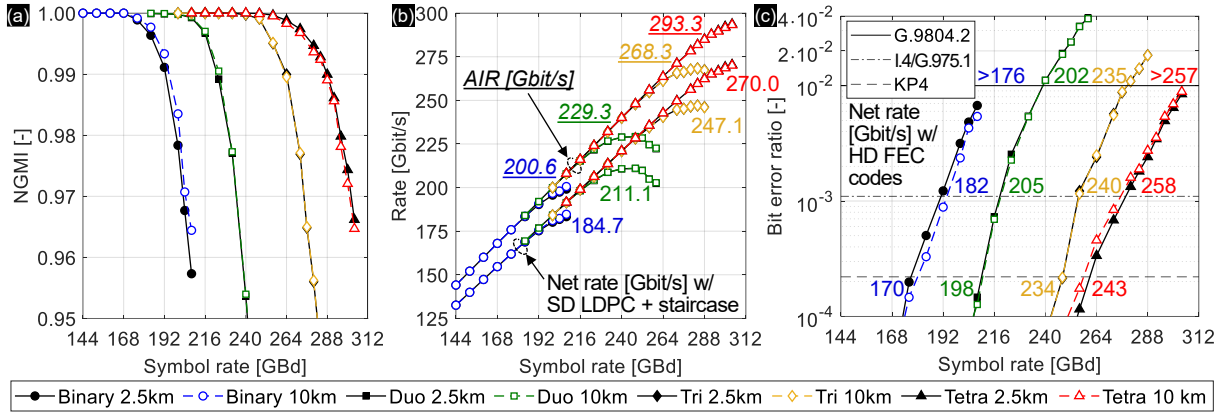


Fig. 3: (a) NGMI; (b) AIR and net bitrate as a function of symbol rate assuming soft-decision inner LDPC; (c) BER and net bitrates assuming various hard-decision FEC schemes.

and M is the number of amplitude levels. The highest AIR after 10 km transmission is 383.6 Gbit/s achieved using 144 GBd PAM-8 signal. The AIR corresponds to the highest information rate that could be achieved with an ideal FEC code. To map the NGMI to the net bitrate that can be achieved with an existing code, we consider an inner soft-decision LDPC code from DVB-S2 family. NGMI thresholds at post-inner-FEC BER of 4.7×10^{-3} are available in^[13]. The LDPC code is serially concatenated with a 6.25%-overhead staircase hard-decision code for a post-outer-FEC BER of 10^{-15} . To achieve fine-grained code rate optimization, we consider punctured and shortened variants of the LDPC mother codes. For a measured NGMI of I_d and a LDPC mother code with NGMI threshold $I_0 > I_d$, the fraction of shortening that can be sustained is calculated as $s = (I_0 - I_d)/(1 - I_d)$ based on mutual information considerations^[14]. Similarly, when $I_0 < I_d$, the amount of puncturing is calculated as $p = (I_d - I_0)/I_d$. For each measured NGMI, we determine in this way the highest code rate that can be supported using punctured or shortened variants of the DVB-S2 codes. The resulting code rates are then used to calculate the net bitrate as $R_b = r_c R_s \log_2(M)$, where r_c is the code rate of the concatenated FEC after optimization of the inner LDPC rate.

As shown in Fig. 2(b), 350.4 Gbit/s net bitrate is achieved with 144 GBd PAM-8 signal obtained using a shortened 8/9 DVB-S2 inner code variant resulting in an overall code rate of 0.811 after the staircase code. For PAM-4 signal, the highest AIR of 300.9 Gbit/s is achieved at 156 GBd, yielding 277.0 Gbit/s net bitrate using a punctured 9/10 DVB-S2 inner code variant resulting in an overall rate of 0.888. Back-to-back results which overlap with 2.5 km results are not shown for clarity of presentation, while 2.5 km and 10 km results nearly overlap in all cases, showing a negligible penalty due to fiber transmission.

Results for (poly)binary modulation

As evident from Fig. 3, polybinay signals can be

used to support transmission at much higher symbol rates compared to a conventional binary modulation thanks to the spectral shaping, which leads to: (i) a reduction of the effective electrical bandwidth and (ii) an increase in the electrical swing driving the modulator. For instance, comparing at NGMI value of 0.97 in Fig. 3(a), binary modulation could operate at 204.5 GBd, duobinary at 233.5 GBd, tribinary at 274.0 GBd and tetrabinary at 300.0 GBd, increasing the symbol rate as well as all other evaluated metrics by nearly 50%. The increment in n leads to the increased number of amplitude levels ($2^n + 1$ levels), yielding 9 levels for $n = 3$, but 17 levels for $n = 4$. The case of $n > 3$ is not considered in this paper due to considerably higher required SNR, which prevents rate improvements. The AIR and net bitrate in Fig. 3(b) are computed in the same way as described in the previous section for PAM signal, and the best result for each modulation format is indicated in Fig. 3(b). For binary and tetrabinary modulation, further improvement in the net bitrate is still possible by increasing the symbol rate, even beyond 304 GBd for tetrabinary modulation.

Fig. 3(c) shows BERs, where bits are hard-decided based on the LLR sign, and assumed to be fed to a HD-input FEC. Three different FEC thresholds are marked. The net bitrates are computed for 10 km transmission at the point of intersection with respective FEC threshold.

Conclusions

By employing an ultrabroad-bandwidth and micron-sized-footprint plasmonic MZM, an ultrahigh symbol rate IM/DD system is experimentally demonstrated. 304 GBd (AIR 293.3 Gbit/s, net 270.0 Gbit/s) polybinary modulation, as well as PAM-8 modulation at 432 Gbit/s (AIR 383.6 Gbit/s, net 350.4 Gbit/s) are successfully received after 10 km of fiber.

Y. Lefevre acknowledges support of the Flemish Government funding agency VLAIO, SPIC project (HBC.2020.2197). Polariton Technologies Ltd. thanks the Binnig and Rohrer Nanotechnology Center (BRNC).

References

- [1] J. D'Ambrosia, "The Case for 1.6 Terabit Ethernet," IEEE 802.3 Beyond 400 Gb/s Ethernet Study Group, May 2021. [Available online] https://www.ieee802.org/3/B400G/public/21_05/dambrosia_b400g_01b_210524.pdf
- [2] C. Minkenberg, R. Krishnaswamy, A. Zilkie, and D. Nelson, "Co-packaged datacenter optics: Opportunities and challenges," *IET Optoelectronics*, vol. 15, no. 2, pp. 77-91, 2021.
- [3] X. Zhou, R. Urata and H. Liu, "Beyond 1 Tb/s Intra-Data Center Interconnect Technology: IM-DD OR Coherent?," in *Journal of Lightwave Technology*, vol. 38, no. 2, pp. 475-484, Jan. 2020, doi: 10.1109/JLT.2019.2956779.
- [4] N.-P. Diamantopoulos *et al.*, "Net 321.24-Gb/s IMDD Transmission Based on a >100-GHz Bandwidth Directly-Modulated Laser," in *Proc. OFC 2020, PDP Th4C.1*.
- [5] S. Yamaoka *et al.*, "Directly modulated membrane lasers with 108 GHz bandwidth on a high-thermal-conductivity silicon carbide substrate," *Nat. Photonics* vol. 15, no. 28, 28–35 (2021), doi: 10.1038/s41566-020-00700-y
- [6] C. Haffner *et al.*, "Low-loss plasmon-assisted electro-optic modulator," *Nature*, vol. 556, no. 7702, pp. 483–486, Apr. 2018.
- [7] H. Mardoyan *et al.*, "222-GBd on-off keying transmitter using ultrahigh-speed 2:1 selector and plasmonic modulator on silicon photonics," in *Proc. ECOC, Dublin, Ireland, Sep. 2019*.
- [8] M. Burla *et al.*, "500 GHz plasmonic Mach-Zehnder modulator enabling sub-THz microwave photonics," *APL Photon.*, vol. 4, no. 5, 2019, Art no. 056106.
- [9] W. Heni *et al.*, "108 Gbit/s Plasmonic Mach-Zehnder Modulator with > 70-GHz Electrical Bandwidth," in *Journal of Lightwave Technology*, vol. 34, no. 2, pp. 393-400, Jan. 2016, doi: 10.1109/JLT.2015.2487560.
- [10] A. Melikyan *et al.*, "High-speed plasmonic phase modulators," *Nat. Photonics* 8, 229–233 (2014), doi: 10.1038/nphoton.2014.9
- [11] C. Haffner *et al.*, "Harnessing nonlinearities near material absorption resonances for reducing losses in plasmonic modulators," *Opt. Mater. Express*, vol. 7, pp. 2168–2181, Jul. 2017.
- [12] P. Kabal and S. Pasupathy, "Partial-Response Signaling," in *IEEE Transactions on Communications*, vol. 23, no. 9, pp. 921-934, Sep. 1975, doi: 10.1109/TCOM.1975.1092918.
- [13] A. Alvarado, E. Agrell, D. Lavery, R. Maher and P. Bayvel, "Replacing the Soft-Decision FEC Limit Paradigm in the Design of Optical Communication Systems," in *Journal of Lightwave Technology*, vol. 33, no. 20, pp. 4338-4352, Oct. 2015, doi: 10.1109/JLT.2015.2450537.
- [14] A. Suls, Y. Lefevre, J. Van Hecke, M. Guenach and M. Moeneclaey, "Error Performance Prediction of Randomly Shortened and Punctured LDPC Codes," in *IEEE Communications Letters*, vol. 23, no. 4, pp. 560-563, Apr. 2019, doi: 10.1109/LCOMM.2019.2900893.